Simulation of a Wind Turbine With Doubly Fed Induction Generator by FAST and Simulink

Conference Paper *in* IEEE Transactions on Energy Conversion · August 2008

DOI: 10.1109/PES.2008.4596027 · Source: IEEE Xplore

3 authors, including:

Roohollah Fadaeinedjad
Graduate University of Advanced Technology
77 PUBLICATIONS **1,396** CITATIONS
SEE PROFILE

M. Moallem
Isfahan University of Technology
168 PUBLICATIONS **4,337** CITATIONS
SEE PROFILE

Simulation of a Wind Turbine With Doubly Fed Induction Generator by FAST and Simulink

Roohollah Fadaeinedjad, *Student Member, IEEE*, Mehrdad Moallem, *Member, IEEE*, and Gerry Moschopoulos, *Member, IEEE*

***Abstract*—In order to fully study the electrical, mechanical, and aerodynamic aspects of a wind turbine with a doubly fed induction generator, a detailed model that considers all these aspects must be used. A drawback of many works in the area of wind turbine simulation is that either a very simple mechanical model is used with a detailed electrical model, or vice versa. Hence, the effects of interactions between electrical and mechanical components are not accurately taken into account. In this paper, three simulation programs—TurbSim, FAST, and Simulink—are used to model the wind, mechanical and electrical parts of a wind turbine, and its controllers. Simulation results obtained from the model are used to observe the interaction of all three factors affecting the operation of a wind turbine system. For example, it is shown how an electrical disturbance can cause dangerous tower vibrations under high speed and turbulent wind conditions, which may not be feasible using a simple model of the wind and wind turbine.**

***Index Terms*—FAST, doubly fed induction generator (DFIG), Simulink, TurbSim, voltage sag, wind energy.**

I. Introduction

WIND energy has been used for thousands of years by humans. Ancient Persians used wind energy to pump water before the birth of Christ [1]. Recently, there has been a growing interest in the use of wind energy as environmental concerns are on the rise. In spite of this growth, more technology advances are needed to make wind energy competitive with many other energy supply methods. Simulation and modeling can be used to study the performance of wind turbine systems.

Considerable research has been done on the modeling and control of wind turbines [2]–[7]. Most of this research, however, has been done using simple mechanical and aerodynamic models of wind turbines that neglect a number of significant characteristics. Research on wind turbines based on more sophisticated mechanical and aerodynamic models has been done only with relatively simple electrical models of the generator, its controllers, and the model of the power system. This is because most researchers who have studied wind turbines have mainly focused on either the electrical or mechanical aspects without paying attention to the operation of the full electromechanical system.

Manuscript received October 30, 2006; revised August 16, 2007. Paper no. TEC-00504-2006.

R. Fadaeinedjad and G. Moschopoulos are with the Department of Electrical and Computer Engineering, University of Western Ontario, London, ON N6A 5B9, Canada (e-mail: rfadaein@uwo.ca; gmoschopoulos@eng.uwo.ca).

M. Moallem is with the School of Engineering Science, Simon Fraser University, Surrey, BC V3T 0A3, Canada (e-mail: mmoallem@sfu.ca).

Color versions of one or more of the figures in this paper are available online at http://ieeexplore.ieee.org.

Digital Object Identifier 10.1109/TEC.2007.914307

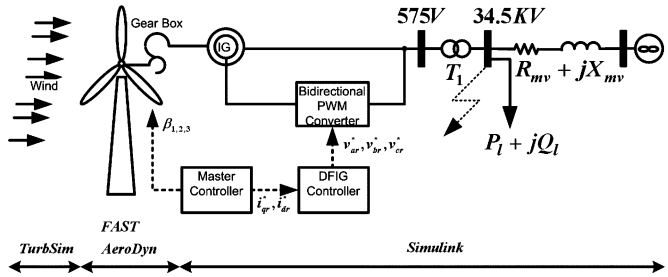

Fig. 1. Simulation structure of the variable speed wind turbine with doubly fed induction generator (DFIG) and grid connection.

Due to an increase in the number and size of wind turbine installations, many utilities request that wind turbines support the grid following disturbances. With this regard, ride through capability of wind turbines is one of the most important subjects, on which considerable research has been done [8]–[13]. Most of the research, however, has been done using relatively simple mechanical and aerodynamic models of wind turbines that neglect a number of significant characteristics from mechanical point of view. It is very important to consider both the electrical and mechanical aspects of wind turbines simultaneously to study overall control performance of the wind turbine systems, especially since an electrical disturbance such as a voltage sag can affect mechanical performance (e.g., can cause vibrations). It is shown that an electrical disturbance can cause severer tower vibrations due to high speed, turbulent wind, which may not be feasible using a simple model of the wind turbine. A detailed model that combines all electrical, mechanical, and aerodynamic aspects of a wind turbine system is therefore needed.

In this paper, it will be shown that a combination of three different simulation packages, namely TurbSim, FAST, and Simulink can be used to model the electrical and mechanical aspects of a wind turbine in detail. The paper will review some wind turbine concepts, along with software tools and a proposed simulation structure. The design of the controllers are described and simulation results are presented.

II. Simulation Structure and Tools

The simulation structure of a variable-speed wind turbine with doubly fed induction generator (DFIG) is shown in Fig. 1. As can be seen, this system consists of a wind turbine with a variable-speed constant frequency DFIG. This means that the stator is directly connected to the grid while the rotor winding is connected via slip rings to an inverter. The inverter is designed so that the induction generator can operate in a limited

variable-speed range. The gear–box ratio is set so that the nominal speed of the induction generator corresponds to the middle value of the rotor speed range of the wind turbine. This is done in order to minimize the size of the inverter that will vary with the rotor speed range.

In this paper, three-dimensional turbulent wind has been simulated by TurbSim [14]. FAST has been used to simulate the mechanical parts of wind turbine, whereby AeroDyn [15] has been used to model the aerodynamic forces [16]. The programs TurbSim, AeroDyn, and FAST have been developed at the National Renewable Energy Laboratory (NREL), Golden, CO (wind.nrel.gov), and are accessible to the public [14]–[16]. The controllers, DFIG, and power system have been modeled by Simulink blocks. The simulation procedure will be explained in the following sections.

III. TurbSim for Simulation of Wind

TurbSim is a stochastic, full field, turbulent wind simulator. It has been developed for simulating of a full-field flow for turbulence structures that reflect the proper space and time turbulent velocity field relationships seen in instabilities associated with nocturnal boundary layer flows [14]. TurbSim provides simulations of advanced turbine designs with simulated inflow turbulence environments that incorporate many of the important fluid dynamic features that are known to adversely affect turbine aeroelastic response and loading.

IV. AeroDyn for Simulation of Aerodynamic Forces

A key element in wind turbine simulation is the calculation of the blade aerodynamic forces since they can cause vibration of the mechanical structure of wind turbine and influence the generated torque (power). In this research, the mechanical torque, deflection, and velocities of the mechanical structure are calculated based on the aerodynamic forces for each part of the blades. The effects of blade deflection and velocities on blade aerodynamic forces are accounted for. These subjects have not been considered in previous works, which have mainly studied the problems from an electrical point of view [2]–[13], [17], [18].

In order to study the forces and moments acting on a wind turbine structure, it is useful to understand the elements of blade aerodynamics. Thus, blade element momentum (BEM) theory is briefly presented in this section [19]. The airflow over a stationary blade causes a lift force F_L and a drag force F_D. As can be seen in Fig. 2, the lift force is perpendicular to the direction of airflow and the drag force is in the direction of airflow. If the airfoil blade moves in the direction of the lift force, it sees the relative velocity W, where the wind velocity is V. The angle α made by the relative wind velocity with the blade chord line is called the angle of attack (AOA). The angle made by the chord line with the plane of rotation is the summation of the twist angle ϕ and the pitch angle β. The lift and drag forces on the blade can be written as $F_L = 0.5\rho c C_L W^2$ and $F_D = 0.5\rho c C_D W^2$, where ρ is density of air, c is the chord length of airfoil section, C_L is the lift coefficient, and C_D is the drag coefficient. Using the BEM theory, the aerodynamic forces are calculated in AeroDyn and passed back to the dynamic subroutines in FAST [15], [16]. The effects of the blade deflection and velocities on blade aerodynamic forces are accounted for in AeroDyn.

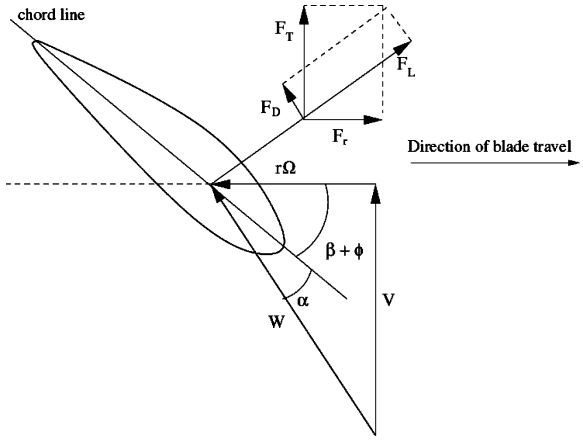

Fig. 2. Aerodynamics of airfoil [19].

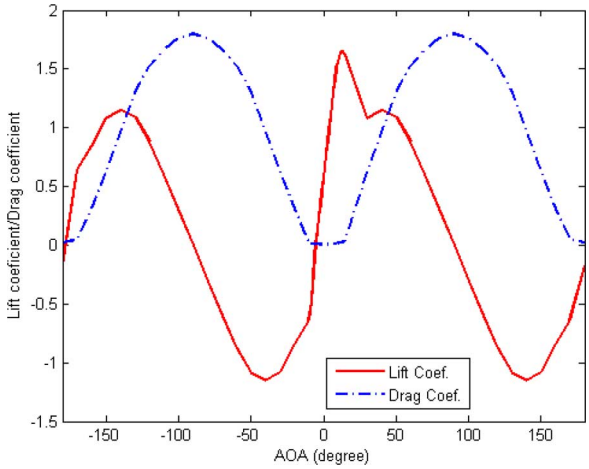

Fig. 3. Variation of C_D and C_L with the AOA

A subroutine package named AeroDyn has been developed at the University of Utah [15], [16]. To use this subroutine, some input data files should be prepared including wind profile, airfoil lift, and drag coefficients and some definable parameters. Some preprocessor software, i.e., FoilCheck and AirfoilPrep, can be used to create the input files for the aerodynamic tables in AeroDyn. In this paper, each blade has been divided into 15 parts and for each part, certain airfoil type, pitch twist angle, and chord length have been defined. The combination of three airfoils, introduced by NREL, is used for the blades. The variation of the lift and drag coefficients with the AOA is shown in Fig. 3.

V. FAST for Simulation of Mechanical Parts of Wind Turbine

Different methods may be used to study the mechanical dynamics of a wind turbine. If the tower, for example, is modeled by a mass-spring model, one cannot calculate the bending and

the mechanical loads on certain parts of the tower. Moreover, this model is not suitable for a flexible structure.

A comprehensive analysis of a flexible structure can be done by software based on finite element methods or similar approaches. In this regard, a program called FAST has been developed [16]. This software is specifically intended for simulating both two- and three-bladed wind turbines. The code uses a modal approach in combination with Kane Dynamics to develop the equations of motion. The code also runs significantly faster than a large comprehensive code such as ADAMS because of the use of the modal approach with fewer degrees of freedoms (DOFs) to describe the most important parts of turbine dynamics. The FAST code can model a three-bladed horizontal axis wind turbine (HAWT) with 24 DOFs.

In this research, FAST has been used to model an upwind, three-bladed rotor HAWT with a rigid hub and foundation, considering 16 of 24 DOFs including first and second flapwise blade mode, edgewise blade mode, drivetrain rotational flexibility, yaw angle, first and second tower fore–aft bending mode, first and second tower side-to-side bending mode, and generator azimuth angle. The DOFs for rotor furl, tail furl, and platform have been neglected, as rotor furl and tail furl are usually used for small wind turbines, and it is assumed that the platform is installed on the ground not on the sea. Using a linear modal representation, FAST models flexible elements, such as the tower and blades. The reliability of this representation depends on the generation of accurate vibration mode shapes, which are input into FAST. A program called BModes [20] can be used to generate these mode shapes. As mentioned before, FAST allows us to specify four different mode shapes, the two fore–aft modes are defined separately from the two side-to-side modes, for the tower. In this paper, however, same mode shapes for fore–aft and side–side bending modes have been used. The mode shapes take the form of a sixth-order polynomial with the zeroth and first terms always being zero. This is because the mode shapes are cantilevered at the base so they must have zero deflection and slope there. At the top of the tower, where the normalized height is 1, the deflection must have a normalized value of 1. This means that the sum of the polynomial coefficients must add to 1. The blade and tower mode shapes that are used in this research have been shown in Figs. 4 and 5. Moreover, some wind turbine principal data can be found in Table II.

The vibration modes can be excited by mechanical or electrical disturbances. For instance, a temporary three-phase fault in the power system can excite the lateral vibration modes of the tower. Sustainable oscillations may happen if the wind turbine remains connected to the network. The severity of these vibrations is influenced by wind turbine operating conditions and power system characteristics. These subjects will be explained in Section VIII-C.

FAST reads mechanical system parameters from some input files and creates some output files, which have been shown in Fig. 6. Moreover, it can be used to exchange data with Simulink [16]. The controller and the electrical parts of a wind turbine can be implemented by Simulink blocks where the wind turbine is simulated by FAST.

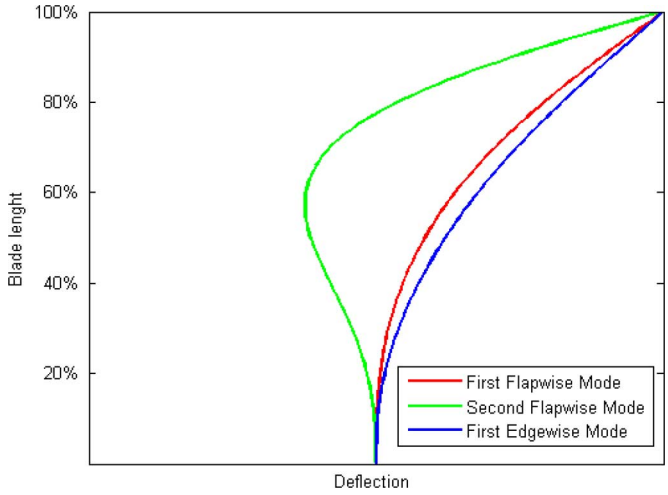

Fig. 4. Blade vibration mode shapes.

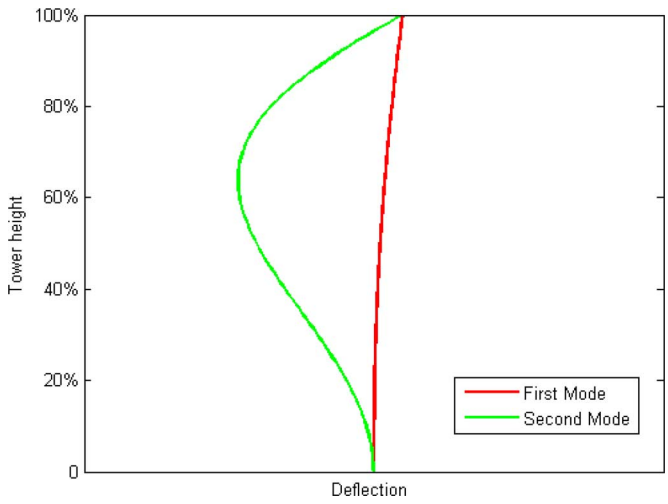

Fig. 5. Tower vibration mode shapes.

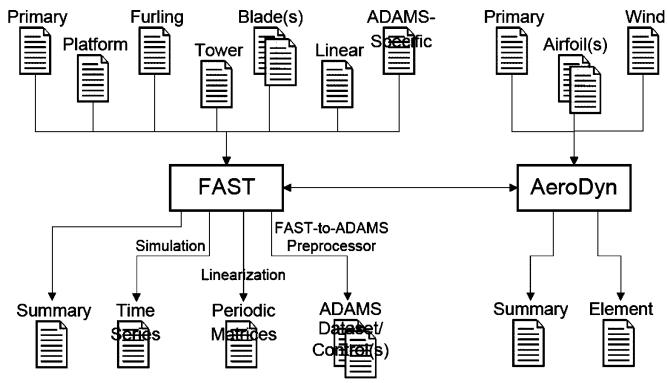

Fig. 6. Input and output files of FAST and AeroDyn [16].

VI. Time-Domain Simulation of the DFIG Connected to the Grid

The time-domain simulation of the DFIG connected to a grid will be explained in this section. The simulation consists of a bidirectional pulsewidth modulation (PWM) converter, the

TABLE I
INDUCTION GENERATOR AND GRID PARAMETERS

Parameter	value
Rated apparent power	$1.5/0.9MVA$
Rated power	$1.5MW$
Rated voltage(line to line)	$0.575kV$
Frequency	$60Hz$
Stator/rotor turns ratio	1
Stator resistance	0.0014Ω
Stator leakage inductance	8.998×10^{-5} H
Rotor resistance	$9.9187 \times 10^{-4}\Omega$
Rotor leakage inductance	$8.2088 \times 10^{-5}H$
Magnetizing inductance	$1.526 \times 10^{-3}H$
Generator inertia about HSS	$53.036kg.m^2$
Pole pairs	3
Transformer rated apparent power	$1.75MVA$
Transformer impedance	$0.0077 + j0.0579pu$
Load power at $34.5kV$ bus	$500kW$
Load power factor	0.8

power system, and an induction machine. In order to link an DFIG model to FAST in a Simulink environment, the model must be expressed in time domain. There is a model for wind turbines with the DFIG in Simulink, but it is not used in this paper because it is in phasor domain [21]. The data for the induction generator and grid connection used in this study are given in Table I.

A. Power System Connection

The simulation study has been conducted on the system shown in Fig. 1, where a local load at 34.5 kV bus is supplied by a wind turbine with an DFIG configuration through a step-up transformer. The power system connection is represented by three constant voltage sources connected in series with its Thevenin equivalent impedance. In other words, the grid connection model is based on short-circuit level (SCL) at point of common coupling (PCC).

B. Bidirectional Converter

Six controlled voltage and current sources with their limiters have been used to model the bidirectional PWM converter. The converter dynamics including switch dynamics have not been considered in this paper.

C. Induction Machine

The induction machine is modeled by Simulink and FAST. Simulink is used to simulate the electrical dynamics of the machine, where FAST models the mechanical dynamics.

The induction machine operates in either generator or motor mode. The mode of operation is dictated by the sign of the mechanical torque T_m. The electrical part of the machine is represented by a fourth-order state–space model. All electrical variables and parameters are referred to the stator. All stator and rotor quantities are in the synchronously rotating reference frame ($d-q$ frame).

The model of the induction machine in Simulink is based on $d-q$ equivalent model, shown in Fig. 7 [22]. To solve the related equations, they can be rearranged in state–space form.

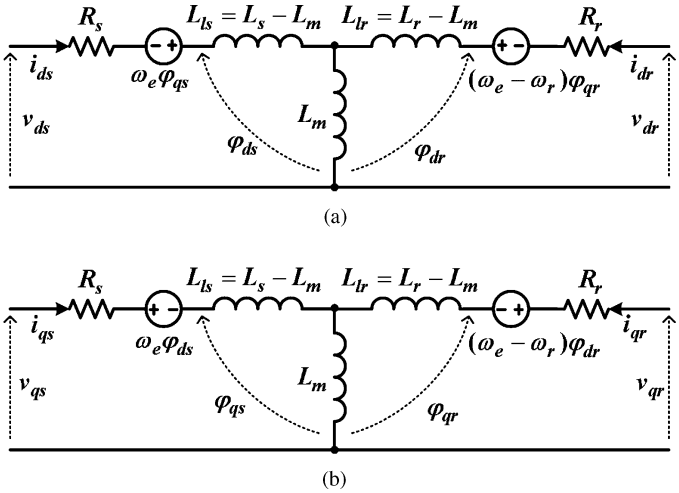

Fig. 7. Dynamic or $d-q$ equivalent circuit of an induction machine at synchronously rotating reference frame [22].

The induction machine modeling equations can be written as

$$\frac{d}{dt}\varphi_{qs} = v_{qs} - \omega_e\varphi_{ds} + \frac{R_s}{\sigma L_s}\left(\frac{L_M}{L_r}\varphi_{qr} - \varphi_{qs}\right) \tag{1}$$

$$\frac{d}{dt}\varphi_{ds} = v_{ds} + \omega_e\varphi_{qs} + \frac{R_s}{\sigma L_s}\left(\frac{L_M}{L_r}\varphi_{dr} - \varphi_{ds}\right) \tag{2}$$

$$\frac{d}{dt}\varphi_{qr} = v_{qr} - (\omega_e - \omega_r)\varphi_{dr} + \frac{R_r}{\sigma L_r}\left(\frac{L_M}{L_s}\varphi_{qs} - \varphi_{qr}\right) \tag{3}$$

$$\frac{d}{dt}\varphi_{dr} = v_{dr} + (\omega_e - \omega_r)\varphi_{qr} + \frac{R_r}{\sigma L_r}\left(\frac{L_M}{L_s}\varphi_{ds} - \varphi_{dr}\right) \tag{4}$$

$$i_{qs} = \frac{1}{\sigma L_s}\varphi_{qs} - \frac{L_M}{\sigma L_r L_s}\varphi_{qr} \tag{5}$$

$$i_{ds} = \frac{1}{\sigma L_s}\varphi_{ds} - \frac{L_M}{\sigma L_r L_s}\varphi_{dr} \tag{6}$$

$$i_{qr} = \frac{1}{\sigma L_s}\varphi_{qr} - \frac{L_M}{\sigma L_r L_s}\varphi_{qs} \tag{7}$$

$$i_{dr} = \frac{1}{\sigma L_s}\varphi_{dr} - \frac{L_M}{\sigma L_r L_s}\varphi_{ds} \tag{8}$$

$$T_e = \frac{1.5pL_M}{\sigma L_s L_r}\left(\varphi_{qs}\varphi_{dr} - \varphi_{ds}\varphi_{qr}\right). \tag{9}$$

For the mechanical part, we have

$$\frac{d}{dt}\omega_r = \frac{p}{J}(T_e - T_m) \tag{10}$$

$$\frac{d}{dt}\theta_r = \omega_r \tag{11}$$

where

d, q	direct and quadrature axis;
r, s	rotor and stator variables;
R_r, R_s	rotor, stator resistance;
L_{lr}, L_{ls}	rotor, stator leakage inductances;
L_r, L_s	rotor and stator inductances;
L_M	magnetizing inductance;
v_{qs}, v_{ds}	q- and d-axis of stator voltages;
i_{qs}, i_{ds}	q- and d-axis of stator currents;

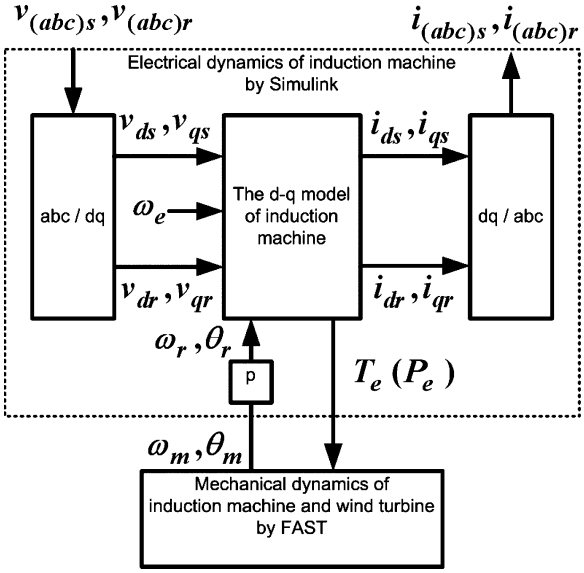

Fig. 8. Simulation of induction machine dynamics by Simulink and FAST.

$v_{qr}, v_{dr}, i_{qr}, i_{dr}$	q- and d-axis of rotor voltage and currents;
$\varphi_{qs}, \varphi_{ds}$	q- and d-axis of stator flux;
$\varphi_{qr}, \varphi_{dr}$	q- and d-axis of rotor flux;
T_e, T_m	electrical and mechanical torque;
θ_r	rotor angular electrical position;
ω_r	rotor angular electrical speed;
θ_m, ω_m	rotor angular position and speed;
ω_e	stator angular electrical frequency;
σ	leakage coefficient;
J	generator and shaft inertia;
p	number of pole pairs.

Assuming a large inertia for the mechanical shaft, ω_r can be considered as a constant in (3) and (4). With this assumption, the mechanical dynamics of generator [(10) and (11)] and involved mechanical parts of wind turbine (gear box, low-speed shaft, and high-speed shaft) have been modeled with more details by FAST in longer time step. The shaft torsional dynamics are considered in FAST, whereas they cannot be modeled by using (10) and (11).

The $d-q$ model requires that all the three-phase variables be transformed into the two-phase rotating frame. Consequently, the induction machine model will have the blocks transforming the three-phase voltages to $d-q$ frame and $d-q$ currents back to the three-phase system, as shown in Fig. 8.

VII. Design Controllers for DFIG and Wind Turbine

Compared to fixed-speed wind turbines, variable-speed wind turbines can extract more power by operating with a controlled tip speed ratio, which will enable maximum power tracking [10], [23]. Wind turbines usually have at least three different possible control actuators: blade pitch, generator torque, and machine yaw. To control a variable-speed wind turbine, it is important to know the relationship between generated power, rotation speed, and wind speed. This is discussed as follows.

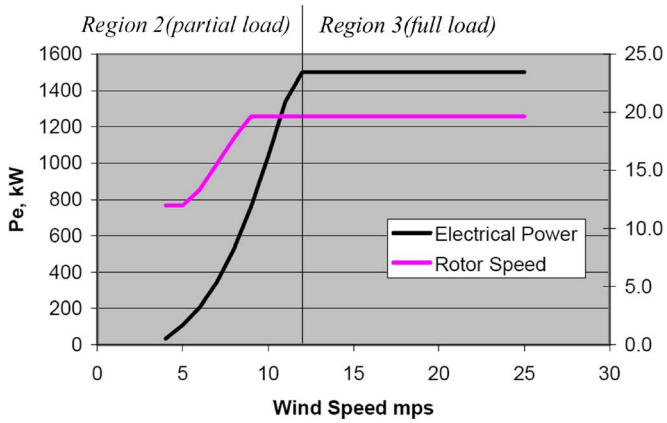

Fig. 9. Power curve and desired rotor speed (low-speed shaft) for wind turbine [24].

The amount of power produced by a turbine can be expressed as $P = 0.5\rho A C_P V^3$, where P is the generated power, A is the area of the rotor disk, and C_P is the power coefficient. The power coefficient C_P is a function of the blade pitch angle β and the tip speed ratio $\lambda = \Omega r/V$, where Ω is the rotor speed and r is the rotor radius. For an optimum energy production strategy, λ and β should be chosen to give an optimum C_P. The turbine should operate at this tip speed ratio, regardless of the wind speed. However, operating wind turbines at the optimum C_P over a large range of wind speeds is not practical.

As mentioned in Section IV, the aerodynamic forces in wind turbines are related to the square of the mean wind speed. At higher wind speeds, the turbine must, therefore, be designed to withstand higher forces, which increases the machine weight and cost. Rated wind speed is the velocity at which maximum output power (rated power) is achieved. For wind speeds above this rated wind speed, power must be held constant by the use of wind turbine controls, or else the power would increase in proportion to the cube of the wind speed and overheat the generator and power electronic system. Fig. 9 shows the power curve of the simulated wind turbine. The area of the curve where $C_{P\max}$ (maximum C_P) is maintained by varying the turbine speed is called region 2 (or partial load). The area in which power is held constant at and above the rated power point is called region 3 (or full load).

Blade pitch, the most effective method of controlling aerodynamic loads, is used to limit the rotation speed above rated wind speed. Generator torque (power) is used not only to maximize the captured power from wind below rated wind speed, but also to limit the captured power above rated wind speed. In addition, the output power of the turbine can be limited by yawing the machine out of the wind, thereby decreasing the projected rotor area A and reducing power. Most often, yaw control is used only to respond to changes in wind direction in an attempt to reduce the yaw error (the angle between the mean wind direction and the direction of orientation of the turbine) and thereby maximize power.

The overall control scheme is shown in Fig. 10. As can be seen, the controller consists of three main parts: the current

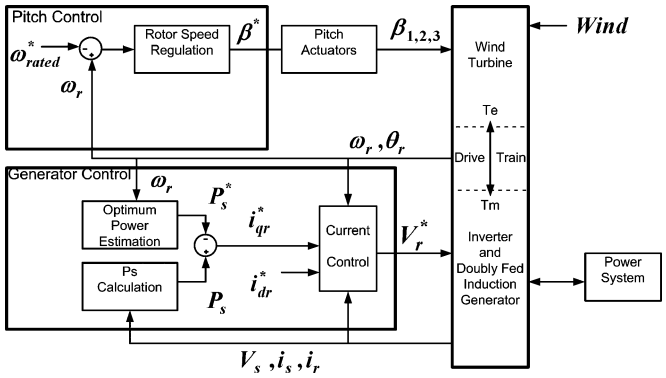

Fig. 10. Overall control structure for wind turbine.

controller, the rotor pitch controller, and the power controller. These parts will be explained in following sections.

A. Pitch Controller

The pitch controller is used to regulate speed in region 3 of operation. Above the rated wind speed, the generated output power will change only in proportion to rotor speed since the torque remains constant; thus, power regulation is entirely dependant upon speed regulation.

A PID controller has been implemented as the pitch controller. The pitch demand is limited to the range of $\beta_{\min}$ to $\beta_{\max}$, where $\beta_{\min}$ is the pitch angle at which optimum rotor aerodynamic performance is achieved, when the rotor speed is below the desired set point ω^*_{rated} in region 2 of operation. An integrator antiwindup must be included in the controller to prevent the windup [25]. The pitch actuator model is a simple second-order system:

$$H(s) = \frac{\beta_{1,2,3}(s)}{\beta^*(s)} = \frac{\omega_n^2}{s^2 + 2\zeta\omega_n s + \omega_n^2} \tag{12}$$

with $\zeta = 80\%$ of critical damping and a natural frequency that is multiple of the rotor speed. In this case, $\omega_n = 4\Omega$ has been used [26].

B. Current Controller (DFIG Controller)

The induction machine is controlled in a synchronously rotating $d-q$ axis frame with the d-axis aligned along the stator flux position. This permits decoupled control of electromagnetic torque and rotor excitation currents. The control method for the DFIG with back-to-back PWM scheme is similar to work by Tapia [7]. The bidirectional PWM converter provides the actuation, and the control requires the measurement of the stator and rotor currents, stator voltages, and the rotor position. Aligning stator flux along d-axis, the induction machine equations may be rewritten as follows

$$|\vec{\varphi_s}| = \varphi_{ds} \Rightarrow L_M |\vec{i_{ms}}| = L_s i_{ds} + L_M i_{dr} \tag{13}$$

$$\varphi_{dr} = L_r i_{dr} + L_M i_{ds} = \frac{L_M^2}{L_s}|\vec{i_{ms}}| + \sigma L_r i_{dr} \tag{14}$$

$$\varphi_{qr} = L_r i_{qr} + L_M i_{qs} = \sigma L_r i_{qr} \tag{15}$$

$$v_{dr} = R_r i_{dr} + \sigma L_r \frac{d}{dt} i_{dr} - \omega_{\text{slip}} \sigma L_r i_{qr} \tag{16}$$

$$v_{qr} = R_r i_{qr} + \sigma L_r \frac{d}{dt} i_{qr} + \omega_{\text{slip}} \left(\frac{L_M^2}{L_s} |\vec{i_{ms}}| + \sigma L_r i_{dr} \right) \tag{17}$$

$$T_e = 1.5p(\varphi_{ds} i_{qs} - \varphi_{qs} i_{ds}) \approx -1.5p \frac{L_M^2}{L_s} |\vec{i_{ms}}| i_{qr} \tag{18}$$

where $|\vec{i_{ms}}|$ is stator magnetizing current space phasor modulus and $\omega_{\text{slip}} = (\omega_e - \omega_r)$ is slip frequency (in radians per second). The current controller structure, based on the aforementioned equations, has been shown in Fig. 11. The following steps are used to implement the control algorithm.

1) Estimation of w_e by a phase-lock loop (PLL) and calculation of $\omega_{\text{slip}} = (\omega_e - \omega_r)$.
2) Three-to-two phase Clark's transformation of measured rotor and stator currents.
3) Estimation of the stator flux linkage space phasor angular position ρ_s with respect to stationary direct axis and stator magnetizing current space phasor modulus $|\vec{i_{ms}}|$. Following [27], the equations are given by

$$\vec{\varphi_s} = L_s \vec{i_s} + L_M \vec{i_r}\, e^{j\theta_r} = L_M \vec{i_{ms}}$$
$$\Rightarrow \vec{i_{ms}} = \frac{L_s}{L_M} \vec{i_s} + \vec{i_r}\, e^{j\theta_r}.$$

$$\begin{aligned} i_{\alpha ms} &= \frac{L_s}{L_M} i_{\alpha s} + i_{Dr}, \quad & i_{Dr} &= i_{\alpha r}\cos\theta_r - i_{\beta r}\sin\theta r \\ i_{\beta ms} &= \frac{L_s}{L_M} i_{\beta s} + i_{Qr}, \quad & i_{Qr} &= i_{\alpha r}\sin\theta_r + i_{\beta r}\cos\theta r \\ |\vec{i_{ms}}| &= \sqrt{i_{\alpha ms}^2 + i_{\beta ms}^2}, \quad & \rho_s &= \arctan\frac{i_{\beta ms}}{i_{\alpha ms}}. \end{aligned} \tag{19}$$

4) Expression of rotor current components i_{Dr} and i_{Qr} in the rotating reference frame aligned to the stator flux-linkage space phasor. These new rotor current components i_{dr} and i_{qr} are calculated by the following equations:

$$i_{dr} = i_{Dr}\cos\rho_s + i_{Qr}\sin\rho_s$$
$$i_{qr} = -i_{Dr}\sin\rho_s + i_{Qr}\cos\rho_s.$$

5) Considering (16) and (17), it is possible to decouple the cross coupling between the d and q components of rotor current, $-\omega_{\text{slip}}\sigma L_r i_{qr}$ in v_{dr} and $\omega_{\text{slip}}\sigma L_r i_{dr}$ in v_{qr}, in the control law used. Furthermore, it is feasible to include a feedforward compensation term $\omega_{\text{slip}} \frac{L_M^2}{L_s} |\vec{i_{ms}}|$ in the control law that will compensate for the tracking error caused by variations of the back electromotive force (EMF).
6) In order to implement the control loop, two identical PI controllers are used. From (16) and (17), the dynamics of the current control loop are given by

$$G(s) = \frac{i_{dr}(s)}{v'_{dr}(s)} = \frac{i_{qr}(s)}{v'_{qr}(s)} = \frac{1}{R_r + \sigma L_r s} \tag{20}$$

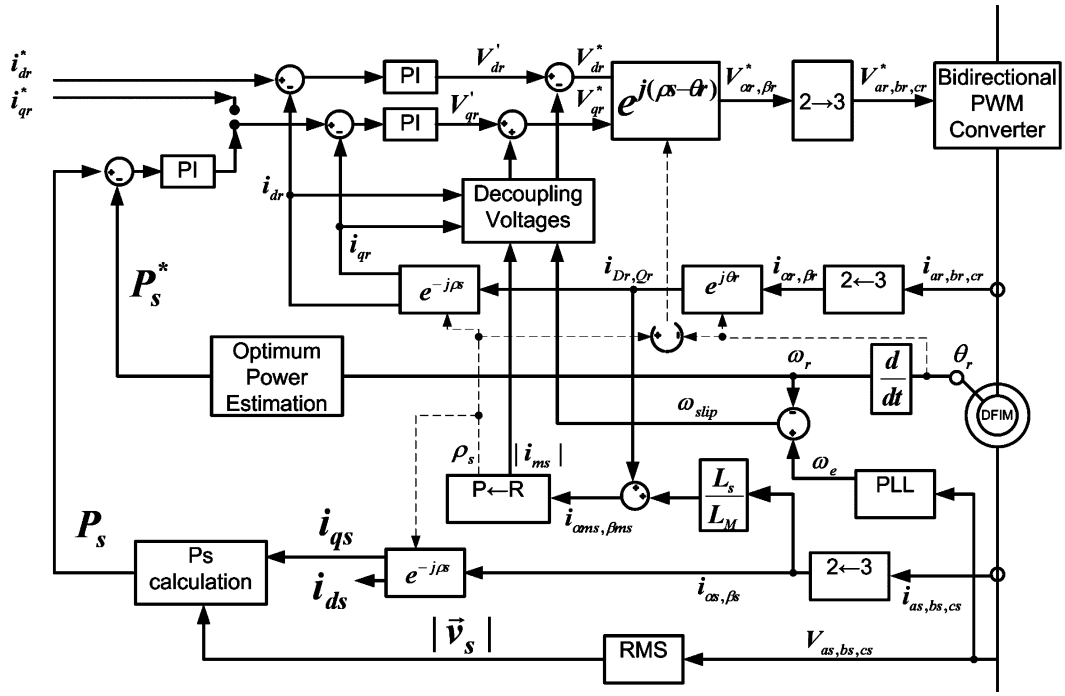

Fig. 11. Current control scheme for the DFIG.

where

$$v'_{dr} = R_r i_{dr} + \sigma L_r \frac{d}{dt} i_{dr} \tag{21a}$$

$$v'_{qr} = R_r i_{qr} + \sigma L_r \frac{d}{dt} i_{qr} \tag{21b}$$

$$v^*_{dr} = v'_{dr} - \omega_{\text{slip}} \sigma L_r i_{qr} \tag{22a}$$

$$v^*_{qr} = v'_{qr} + \omega_{\text{slip}} \left(\frac{L_M^2}{L_s} |\vec{i_{ms}}| + \sigma L_r i_{dr} \right). \tag{22b}$$

Internal mode control (IMC) is used to design the controller [28]. For a first-order system, the controller becomes a PI controller when the IMC is used. Then, we can write:

$$C(s) = \frac{\alpha_c}{s} G^{-1}(s) = k_p + \frac{k_i}{s} \tag{23}$$

where α_c is a design parameter, which is the desired closed-loop bandwidth. The active resistance method has been used to have more damping for disturbance and variations on back EMF in this paper [8]. Thus, k_p and k_i can be written as

$$k_p = \alpha_c(\sigma L_r), \qquad k_i = \alpha_c(R_r + R_a) \tag{24}$$

where R_a is the active resistance. Moreover, antiwindup compensation should be used to prevent the saturation of the converter.

7) Transformation of rotor voltage components from $d-q$ frame to $\alpha-\beta$ frame are as follows

$$v^*_{\alpha r} = v^*_{dr} \cos(\rho_s - \theta_r) - v^*_{qr} \sin(\rho_s - \theta_r) \tag{25}$$

$$v^*_{\beta r} = v^*_{dr} \sin(\rho_s - \theta_r) + v^*_{qr} \cos(\rho_s - \theta_r). \tag{26}$$

8) Two-to-three phase Clark's reverse transformation of rotor voltage components $v^*_{\alpha r}, v^*_{\beta r}$.

The terms i^*_{qr} and i^*_{dr} are applied to the current controller as setting values. The q component of the rotor current i^*_{qr} will be used to control the torque, but the d component of the current i^*_{dr} can be used to achieve unity power factor. If the d component of the rotor current is controlled as

$$i^*_{dr} = \frac{|\vec{\varphi_s}|}{L_M} \approx \frac{V_s}{\omega_e L_M} \tag{27}$$

the unity power factor at the stator is achieved [8]. The term i^*_{qr} may be set to the following value to control the torque

$$i^*_{qr} = -\frac{\omega_e L_s T^*_e}{1.5 p L_M V_s}. \tag{28}$$

However, i^*_{qr} has been calculated by the power controller in this paper.

C. Power Controller

The stator power can be controlled in cascade with current if the current dynamics are set much faster than the power dynamics. The steps followed by the designed control algorithm are summarized as follows.

1) Calculation of stator voltage space phasor modulus $|\vec{v_s}|$.
2) Expression of stator current components, $i_{\alpha s}$ and $i_{\beta s}$, in the rotating reference frame aligned to the stator flux-linkage space phasor. These new stator current components, i_{ds} and i_{qs}, are calculated by the following equations:

$$i_{ds} = i_{\alpha s} \cos\rho_s + i_{\beta s} \sin\rho_s$$

$$i_{qs} = -i_{\alpha s} \sin\rho_s + i_{\beta s} \cos\rho_s.$$

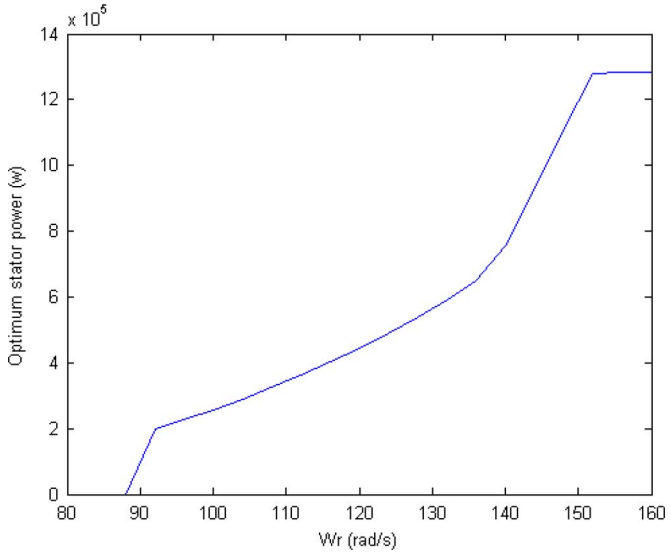

Fig. 12. Relation between optimum stator power P_s^* and ω_r.

3) Computation of stator power P_s using following equation

$$P_s = \frac{3}{2}|\vec{v_s}|i_{qs}. \tag{29}$$

4) Calculation of optimum stator active power P_s^* to be generated from rotor angular speed ω_r. As mentioned in Section VII, the optimum λ should be chosen to capture the maximum wind energy in operating region 2. The relation between optimum stator power setting P_s^* and ω_r is shown in Fig. 12.
5) Implementation of a PI controller to provide the power control loop in order to generate the reference rotor current component i_{qr}^*. A limiter and an antiwindup compensator must be included in this controller.

VIII. Results

It is important to have detailed models of both mechanical and electrical parts of a wind turbine to study certain key issues. The controller's performance are evaluated and the effects of an electrical disturbance on the mechanical parts of wind turbine are studied in the following sections.

A. Controller's Performance

Fig. 13 shows how the pitch controller regulates rotation speed around the rated value $\omega_{\text{rated}}^* = 156.2$ rad/s, in spite of wind speed variation, measured at nacelle height. As can be seen in Fig. 13, the electrical torque is maintained at its rated value.

Fig. 14 shows how the stator active power P_s is controlled at rated value, where the stator reactive power Q_s is maintained close to zero to achieve unity power factor. As can be seen in Fig. 14, there are small fluctuations on rotor active power P_r and total output power P_t caused by wind speed variations.

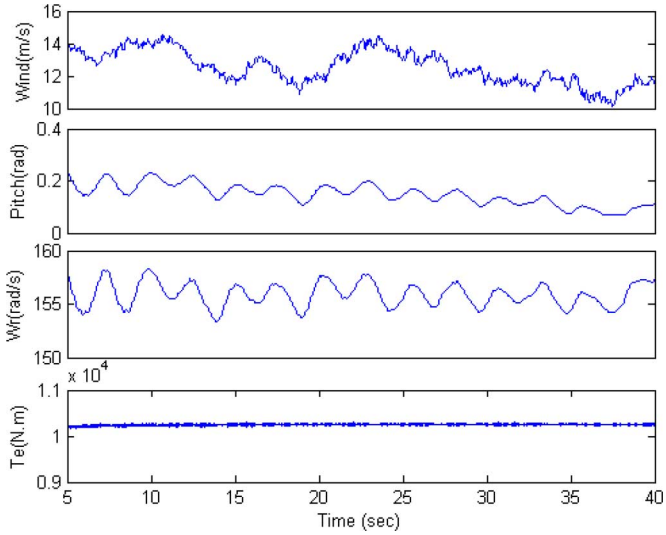

Fig. 13. Wind speed, pitch angle, rotation speed, and electrical torque.

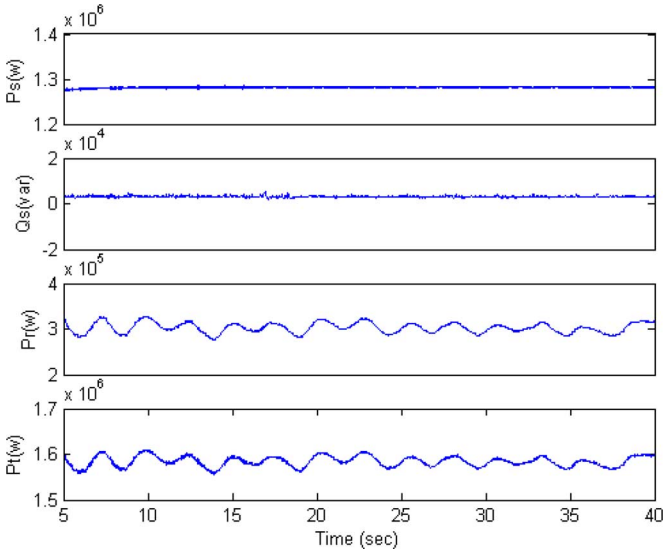

Fig. 14. Stator active and reactive powers, rotor active power, and total output power.

B. Impact of Voltage Sag on Wind Turbine Systems

The effects of an electrical disturbance, voltage sag, on the mechanical response of a wind turbine are studied in this section. The stator voltage and current signals are shown in Fig. 15. The stator voltages sag to 50% at $t = 15$ s and recover to normal voltage level at $t = 15.6$ s. As can be seen in Fig. 15, the voltage sag creates some transients on the stator and rotor currents and the rotor voltage. However, the situation after this voltage sag is not serious enough to trigger the rotor protection devices. The control schemes of the DFIG operate as normal and try to restore the wind turbine's normal operation after the disturbance is cleared.

The voltage and currents transients significantly change the generator active and reactive powers, which are shown in Fig. 16. The lateral tower acceleration, generator torque, and the low-speed shaft twist angle are shown in Fig. 17. Fig. 17 also shows

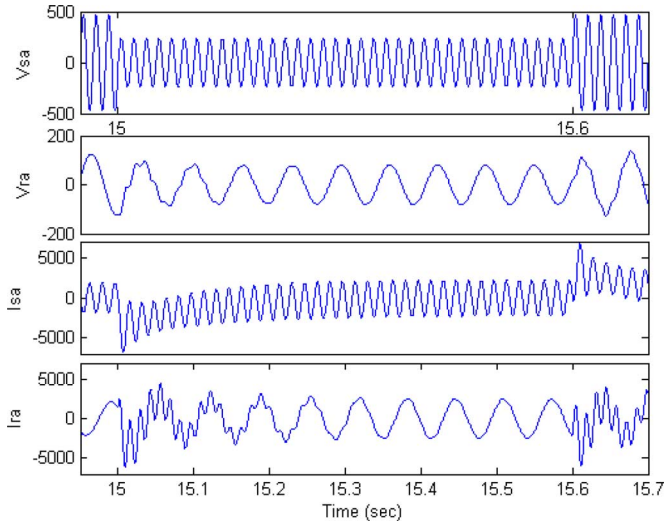

Fig. 15. Voltage and currents of stator and rotor (phase A).

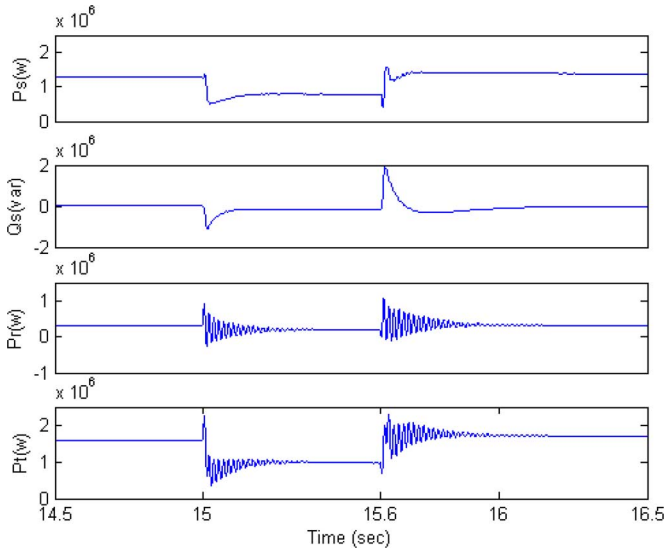

Fig. 16. Effect of 50% voltage sag at the PCC on stator active and reactive powers, rotor active power, and total output power.

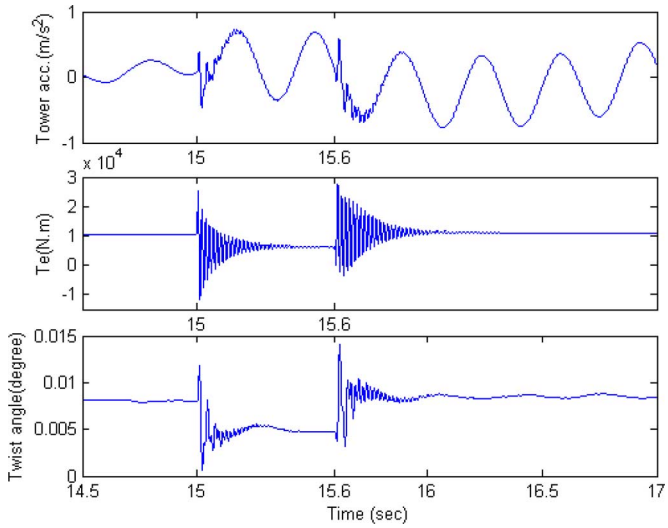

Fig. 17. Effect of voltage sag on lateral tower acceleration, generator torque, and low-speed shaft twist angle.

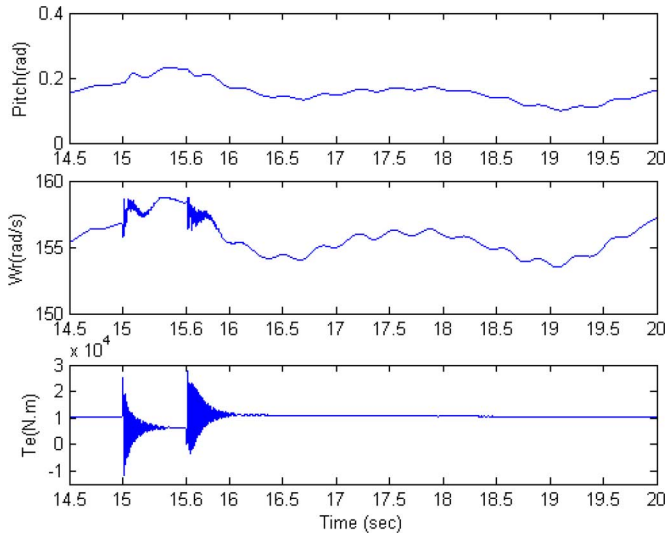

Fig. 18. Effect of voltage sag on pitch controller, rotation speed, and generator torque.

how an electrical disturbance causes vibration and transient forces on the tower. In addition, the shaft twist angle shows how the disturbance may create problems for the shaft.

As can be seen in Fig. 18, the voltage sag rapidly reduces the generator torque, and thus, the rotation speed will be increased, where the pitch controller try to keep that constant.

C. Lateral Tower Vibration Caused by an Electrical Disturbance

As mentioned in Section V, the tower vibration modes can be excited by mechanical or electrical disturbances. In this section, it is shown that an electrical disturbance can cause the wind turbine tower vibration.

1) Impact of A Three-Phase Fault on Tower Vibration: In this study, a resistive, three-phase, temporary fault with duration of six-cycle is applied to the 34.5 kV bus at $t = 15$ s, while the wind turbine is generating rated power at unity power factor. The SCL and X/R ratio of the power system connection have been considered 50 MVA and 5, respectively.

The lateral tower acceleration is shown in Fig. 19. As can be seen, the disturbance causes tower vibration with two different frequencies (i.e., 3 Hz and 0.4 Hz). These frequencies correspond to two different lateral tower vibration modes shown in Fig. 5. The severity of these vibrations is influenced by wind turbine operating conditions (i.e., wind speed) and power system characteristics (i.e., the SCL). These subjects are discussed in following sections.

2) Impact of Wind Speed on Tower Vibration: The tower oscillations, caused by an electrical disturbance, will be severer when wind turbine is working in higher speed and more turbulent wind. An electrical disturbance identical to that of Section VIII-C1 is applied to the network. In this case, however, the wind

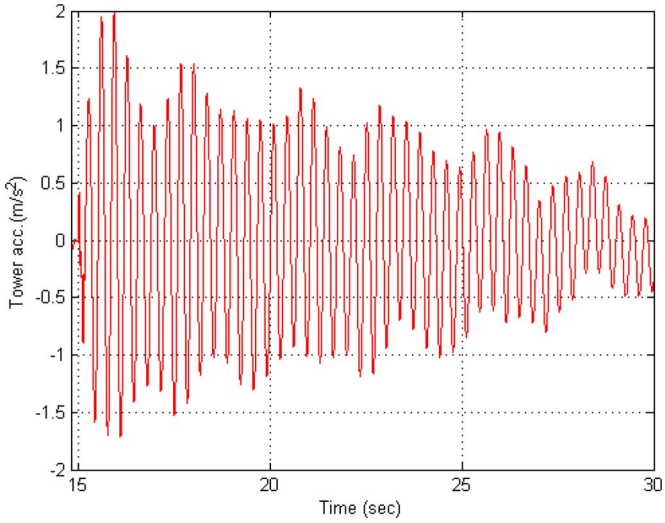

Fig. 19. Effect of the electrical disturbance on the tower acceleration.

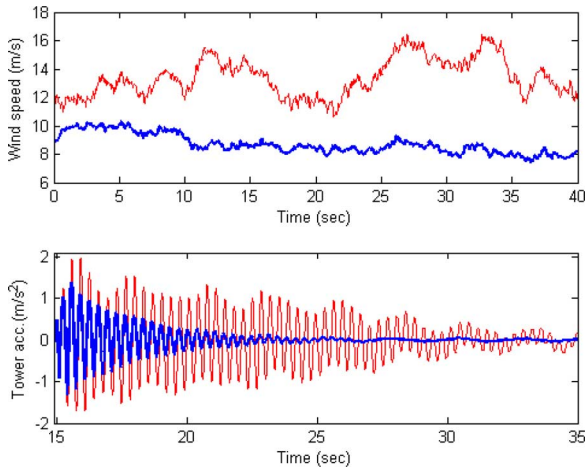

Fig. 20. Effect of the electrical disturbance on the lateral tower acceleration at low-speed (thick) and high-speed (thin) winds.

turbine is subjected to a lower speed and smoother wind distribution. Initially, the wind turbine operates below rated wind speed and generates 740 kW at unity power factor. The system is then subjected to a three-phase fault at $t = 15$ s. The wind speeds at nacelle height and the tower accelerations are shown in Fig. 20 for two different wind distributions. It can be concluded from this figure that the disturbance can cause more dangerous and persistent tower vibration at the higher speeds and more turbulent wind than at lower speeds. As mentioned in Section IV, higher speed wind produces stronger mechanical forces. These forces, themselves, can cause vibration of the mechanical structure, especially blades and tower [29].

3) Impact of Network SCL on Tower Vibration: The power system strength (SCL) has a significant influence on tower vibration caused by an electrical disturbance, which is studied in this section.

In order to study the role that the SCL has on the tower vibration, a fault identical to that of Section VIII-C1 is applied to power system with same wind turbine operating conditions, while the network SCL is varied from 200 to 25 MVA. The lateral tower accelerations for different network SCLs are shown

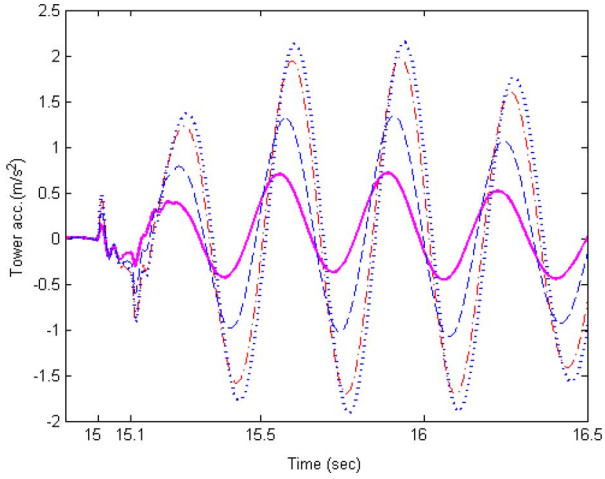

Fig. 21. Effect of the electrical disturbance on the tower acceleration with different network SCL (MVA): 200(–), 100(- -), 50(-.), 25(. . .).

TABLE II
PRINCIPAL DATA OF WIND TURBINE

Parameter	value
Rotor diameter	$70m$
Cut-in wind speed	4 m/s
Cut-out wind speed	25 m/s
Rated wind speed	12 m/s
Rated rotor speed	$19.7rpm$
Tower height	$82.39m$
Tower damping ratio	1.435
Hub radius	$1.75m$
Tilt angle	$5.0°$
Blade pitch angle range	$4° - 90°$
Cone angle	$0.0°$
Blade type	$S818, S825, S826$
Hub mass less blades	$15148kg$
Blade mass	$3912kg$
Nacelle mass	$51170kg$
Blade number	3
Hub inertia about rotor axis (includes blades and LSS)	$34.6 \times 10^3 kg.m^2$
Drivetrain torsional damper	$1.0 \times 10^7 Nm/s$
Drivetrain torsional spring	$5.6 \times 10^9 Nm/rad$
Gearbox ratio	75.7098

in Fig. 21. As can be seen in this figure, the tower vibration magnitude is significantly increased by decreasing the SCL. In other words, the disturbance causes severer tower vibration, when wind turbine is connected to a weaker power system. The X/R ratio of the power system connection have been considered 5 in this case.

IX. CONCLUSION

It was shown that TurbSim, FAST, and Simulink can be used to model the aerodynamic, mechanical, and electrical aspects of a wind turbine with the DFIG in detail. In addition, the results illustrate the relationship between an electrical disturbance and mechanical loads. As shown in Section VIII, having a complete model of the wind turbine system is important to study the overall control performance of wind turbine systems. An important point to consider is that a power system disturbance can cause mechanical problems, which have not been studied in previous works [10]–[13].

Development of new control strategies to tackle problems such as vibration and ride through, and the mechanical phenomena that affect electrical quantities such as output power and voltage are subjects of ongoing and future work.

REFERENCES

[1] *National Resources Canada*. (Jul. 2000). The history of wind energy , [Online]. Available: http://www.canren.gc.ca/

[2] C. Eisenhut, F. Krug, C. Schram, and B. Klockl, "Wind-turbine model for system simulations near cut-in wind speed," *IEEE Trans. Energy Convers*., vol. 22, no. 2, pp. 414–420, Jun. 2007.

[3] D. S. L. Dolan and P. W. Lehn, "Simulation model of wind turbine 3p torque oscillations due to wind shear and tower shadow," *IEEE Trans. Energy Convers*., vol. 21, no. 3, pp. 717–724, Sep. 2006.

[4] C. V. Moreno, J. U. Garcia, and H. A. Duarte, "A frequency domain approach to wind turbines for flicker analysis," *IEEE Trans. Energy Convers*., vol. 18, no. 2, pp. 335–341, Jun. 2003.

[5] C. V. Moreno, H. A. Duarte, and J. U. Garcia, "Propagation of flicker in electric power networks due to wind energy conversions systems," *IEEE Trans. Energy Convers*, vol. 17, no. 2, pp. 267–272, Jun. 2002.

[6] R. Pena, J. C. Clare, and G. M. Asher, "A doubly fed induction generator using back to back PWM converters supplying an isolated load from a variable speed wind-energy generation," *Proc. Inst. Electr. Eng. Electron. Power Appl.*, vol. 143, no. 3, pp. 231–241, May 1996.

[7] A. Tapia, G. Tapia, J. X. Ostolaza, and J. R. Saenz, "Modeling and control of a wind turbine driven doubly fed induction generator," *IEEE Trans. Energy Convers*., vol. 18, no. 2, pp. 194–204, Jun. 2003.

[8] A. Petersson, L. Harnefors, and T. Thiringer, "Evaluation of current control methods for wind turbine using doubly fed induction machines," *IEEE Trans. Power Electron*., vol. 20, no. 1, pp. 227–235, Jan. 2005.

[9] F. Zhou, G. Joos, and C. Abbey, "Voltage stability in weak connection wind farms," in *Power Engineering Society General Meeting*, vol. 2, San Francisco, CA: IEEE, Jun. 2005, pp. 1483–1488.

[10] J. Morren and S. W. H. de Haan, "Ride-through of wind turbines with doubly-fed induction generator during a voltage dip," *IEEE Trans. Energy Convers*., vol. 20, no. 2, pp. 435–441, Jun. 2005.

[11] C. Chompoo-inwai, C. Yingvivatanapong, K. Methaprayoon, and W.-J. Lee, "Reactive compensation techniques to improve the ride-through capability of wind turbine during disturbance," *IEEE Trans. Ind. Appl*., vol. 41, no. 3, pp. 666–672, May/Jun. 2005.

[12] A. Petersson, S. Lundberg, and T. Thiringer, "A DFIG wind turbine ride-through system influence on the energy production," *Wind Energy*, vol. 8, no. 3, pp. 251–263, Jul. 2005.

[13] Y. Lei, A. Mullane, G. Lightbody, and R. Yacamini, "Modeling of the wind turbine with a doubly fed induction generator for grid integration studies," *IEEE Trans. Energy Convers*., vol. 21, no. 1, pp. 257–264, Mar. 2006.

[14] B. J. Jonkman and M. L. J. Buhl. (2007, Apr.). TurbSim User'S Guide. National Renewable Energy Laboratory (NREL), Golden, CO, Tech. Rep. NREL/TP-500-41136, [Online]. Available: http://wind.nrel.gov/ designcodes/preprocessors/turbsim/

[15] P. J. Moriarty and A. C. Hansen. (2005, Dec.). AeroDyn Theory Manual. National Renewable Energy Laboratory (NREL), Golden, CO, Tech. Rep. NREL/TP-500-36881, [Online]. Available: http://wind.nrel.gov/designcodes/simulators/aerodyn/

[16] J. M. Jonkman and M. L. J. Buhl. (2005, Aug.) FAST User'S Guide. National Renewable Energy Laboratory (NREL), Golden, CO, Tech. Rep. NREL/EL-500-38230, [Online]. Available: http://wind.nrel.gov/designcodes/simulators/fast/

[17] R. K. Varma and S. Auddy, "Mitigation of subsynchronous oscillations in a series compensated wind farm with static var compensator," in *Proc. IEEE Power Eng. Soc. General Meeting*, Montreal, QC, Canada, Jun. 2006, pp. 1–7, Paper 1-4244-0493-2/06.

[18] A. Tabesh and R. Iravani, "Small-signal dynamic model and analysis of a fixed-speed wind farm a frequency response approach," *IEEE Trans. Power Del*., vol. 21, no. 2, pp. 778–787, Apr. 2006.

[19] T. Burton, D. Sharpe, N. Jenkins, and E. Bossanyi, *Wind Energy Handbook*. New York: Wiley, 2001.

[20] G. S. Bir. (2006, Feb.). User's Guide to BModes (Software for Computing Rotating Beam Coupled Modes). Golden, CO, Tech. Rep. Draft, [Online]. Available: http://wind.nrel.gov/designcodes/preprocessors/bmodes/

[21] *Power System Blockset for Use With Simulink (User's Guide)*. The Mathworks Inc., Natick, MA, 2004.

[22] B. K. Bose, *Modern Power Electronics and AC Drives*. Upper Saddle River, NJ: Prentice-Hall, 2002, pp. 56–74.

[23] G. Poddar, A. Joseph, and A. K. Unnikrishnan, "Sensorless variable-speed controller for existing fixed-speed wind power generator with unity-power-factor operation," *IEEE Trans. Ind. Electron*., vol. 50, no. 5, pp. 1007–1015, Oct. 2003.

[24] R. Fadaeinedjad, G. Moschopoulos, and M. Moallem, "Simulation of a wind turbine with doubly-fed induction machine using FAST and Simulink," in *Proc. IEEE Int. Symp. Ind. Electron. ISIE 2006*, Montreal, QC, Canada, Jul., pp. 2648–2653.

[25] B. Wittenmark, K. J. Astrom, and K. E. Arzen, "Computer control: An overview," in *Proc. IFAC Professional Brief*. Lund, Sweden: Dept. Autom. Control, Lund Inst. Technol., 2003.

[26] C. Hansen, "Pitch control systems for the windpact rotor design study," Windward Engineering LLC, Salt Lake City, UT, Tech. Rep., Mar. 2001.

[27] P. Vas, *Sensorless Vector and Direct Torque Control*. New York: Oxford Univ. Press, 1998.

[28] L. Harnefors and H. P. Nee, "Model-based current control of ac machines using the internal model control method," *IEEE Trans. Ind. Appl*., vol. 34, no. 1, pp. 133–141, Jan./Feb. 1998.

[29] J. Manwell, J. McGowan, and A. Rogers, *Wind Energy Explained—Theory Design and Application*. New York: Wiley, 2002.

Roohollah Fadaeinedjad (S'06) was born in Kerman, Iran, in 1969. He received the B.S. degree in electrical engineering from Shiraz University, Shiraz, Iran, in 1992, and the M.Sc degree in electrical engineering from Isfahan University of Technology, Isfahan, Iran, in 1995. He is currently working toward the Ph.D. degree in the Department of Electrical and Computer Engineering, University of Western Ontario (UWO), London, ON, Canada.

From 1996 to 1999, he was with Shahid Bahonar University, Kerman, Iran, as a Lecturer. From 1999 to 2004, he was with the Protection and Control Departments of Kerman Regional Electric Company (KREC) and Rasanir Company as a Senior Protection Engineer and a Project Manager. His current research interests include wind energy, control systems, power electronics, and power system protection.

Mehrdad Moallem (M'95) received the B.Sc. degree in electrical and electronic engineering from Shiraz University, Shiraz, Iran, in 1986, the M.Sc. degrees in electrical and electronic engineering from Sharif University of Technology, Tehran, Iran, in 1988, and the Ph.D. degree in electrical and computer engineering from Concordia University, Montreal, QC, Canada, in 1997.

From 1997 to 1999, he was a Postdoctoral Fellow at Concordia University and a Research Fellow at Duke University, Durham, NC. He was with the Department of Electrical and Computer Engineering, University of Western Ontario (UWO), London, ON, Canada, and an Associate Scientist at the Canadian Surgical Technologies and Advanced Robotics (CSTAR) Research Group at the UWO from 1999 to 2007. He is currently an Associate Professor at Simon Fraser University, Surrey, BC, Canada.

Dr. Moallem is a Registered Professional Engineer in the province of Ontario.

Gerry Moschopoulos (S'89–M'98) received the B.Eng., M.A.Sc., and Ph.D. degrees from Concordia University, Montreal, QC, Canada, in 1989, 1992, and 1997, respectively, all in electrical engineering.

From 1996 to 1998, he was a Design Engineer in the Advanced Power Systems Division, Nortel Networks, Lachine, QC, Canada. From 1998 to 2000, he was a Postdoctoral Fellow at Concordia University, where he was engaged in research in the area of power electronics for telecommunications applications. He is currently an Associate Professor at the University of Western Ontario, London, ON, Canada.

Dr. Moschopoulos is a Registered Professional Engineer in the province of Ontario.